Journal of Solid State Chemistry 322 (2023) 123952

Contents lists available at ScienceDirect

Journal of Solid State Chemistry

journal homepage: www.elsevier.com/locate/jssc

Electronic structure characterization of TiO_2-II with the α-PbO_2 structure by electron-energy-loss-spectroscopy and comparison with anatase, brookite, and rutile

Alisa Gordeeva [a], Thomas Thersleff [a], Ying-Jui Hsu [b], Christian Liebske [c], Peter Ulmer [c], Ove Andersson [b], Ulrich Häussermann [a,*]

[a] Department of Materials and Environmental Chemistry, Stockholm University, SE-106 91, Stockholm, Sweden
[b] Department of Physics, Umeå University, SE-901 87, Umeå, Sweden
[c] Institute of Geochemistry and Petrology, ETH Zürich, Clausiusstrasse 25, CH-8092, Zürich, Switzerland

A B S T R A C T

TiO_2-II is a high pressure form of titania with a density about 2% larger than that of rutile. In contrast to the common polymorphs anatase, brookite and rutile its electronic structure and optical properties are poorly characterized. Here we report on a comparative electron-energy-loss-spectroscopy (EELS) study for which high resolution valence-loss and core-loss EELS data were acquired from nanocrystalline (<75 nm sized) titania particles with an energy resolution of about 0.2 eV. Electronic structure features revealed from titanium $L_{3,2}$ and oxygen *K* electron energy loss near-edge structures show a strong similarity of TiO_2-II with both rutile and brookite, which is attributed to similarities in the connectivity of octahedral TiO_6 units with neighboring ones. From combined valence-loss EELS and UV-VIS diffuse reflectance spectroscopy data the band gap of TiO_2-II was determined to be indirect and with a magnitude of ~3.18 eV, which is very similar to anatase (indirect, ~3.2 eV), and distinctly different from rutile (direct, ~3.05 eV) and brookite (direct, ~3.45 eV).

1. Introduction

Titania (TiO_2) exists in various polymorphs of which the tetragonal rutile phase is considered the ground state [1,2]. In addition, anatase and brookite occur in nature. Rutile, anatase, and brookite can be synthesized in the form of crystals, fine particles and as various nanomaterials from solution routes, especially through sol-gel or hydrothermal processing [3,4]. Considerable efforts have been directed to investigate the effect of polymorphic phase, degree of crystallinity, morphology, surface area and size of particles on the various interesting properties and applications of TiO_2, which include solar energy harvesting and hydrogen generation from photochemical reactions [5–7].

In this respect it is interesting to also consider the high pressure polymorph TiO_2-II which adopts the orthorhombic α-PbO_2 type structure [8] because it can be retained at ambient conditions [9]. In the titania phase diagram TiO_2-II is adjacent to rutile [10]. Its bulk synthesis is achieved quantitatively and within hours when hydrothermally converting amorphous TiO_2 or rutile in the pressure range 5–6 GPa [11,12]. The conversion of amorphous TiO_2 particles occurs at rather low temperatures, 250–350 °C, and affords 10 nm–0.1 μm sized crystals [12], whereas the conversion of bulk (submicron-sized) rutile requires temperatures around 650 °C for appreciable kinetics, leading to micron-sized crystals [11]. The phase boundary between rutile and TiO_2-II at temperature above 500 °C has been determined from both experiments and thermodynamic calculations [10,13,14].

The comparatively low pressure conditions required for the preparation of TiO_2-II would make it accessible by industrial high pressure processing. Larger quantity batches of pure TiO_2-II can also be obtained from shock synthesis [15]. Further, metastable TiO_2-II has been prepared under the non-equilibrium conditions of "stagnating flame" synthesis [16,17], although only as a 70/30% mixture with rutile, and TiO_2-II has been reported as intermediate in high-energy ball milling of anatase [18,19]. Interestingly, TiO_2-II can also be obtained with low yields (<10%) when dissolving Ti_3O_5 in sulfuric acid at elevated temperatures [20]. Finally, TiO_2-II can be grown as thin films, using atomic layer deposition on sapphire and Si substrates [21,22].

The optical, electrical, and catalytic properties of TiO_2-II have not yet been well characterized [23]. Most knowledge stems from theoretical calculations [24–26]. In this manuscript we report a comparative electron-energy-loss-spectroscopy (EELS) study of all four TiO_2 polymorphs. The electron-loss near edge structure (ELNES) from core-loss EELS reflects the electronic structure and coordination environment of

* Corresponding author.
E-mail address: Ulrich.Haussermann@mmk.su.se (U. Häussermann).

https://doi.org/10.1016/j.jssc.2023.123952
Received 4 January 2023; Received in revised form 23 February 2023; Accepted 1 March 2023
Available online 2 March 2023

the corresponding excited atoms (i.e. Ti and O) whereas valence-loss EELS (VEELS) probes the band gap. A compilation of high energy resolved EELS data for all four polymorphs will also proof useful for research concerned with the analysis of mixed phase samples by high precision nanophase mapping and/or the study of core-shell and grain boundary situations [27–33].

2. Methods

Samples. The materials employed for this investigation were nanocrystalline brookite, rutile, TiO_2-II and anatase. The three former were obtained from the hydrothermal conversion of amorphous TiO_2 in a high pressure hydrothermal environment (see supporting information for details). Anatase (99.8%, nanopowder) was purchased from Sigma-Aldrich. All materials were pure single-phase as confirmed by powder X-Ray diffraction data (see supporting information, Fig. S1). Investigated particles were between ~15 and ~75 nm in lateral size and <30 nm in thickness (as estimated from low loss EELS data [34], see supporting information, Fig. S2).

Electron energy loss spectroscopy. Valence-loss EELS data were acquired in monochromated STEM mode on a Themis Z TEM equipped with probe and image aberration correctors. The instrument was operated at 300 kV accelerating voltage with a dispersion of 10 meV/channel. The convergence and collection angles were 21.4 mrad and 23 mrad, respectively. The probe current was estimated to be 400 pA. Under these conditions the zero-loss elastic peak (instrument response function or ZLP) full width half maximum (FWHM) was typically 0.22 eV. The probe was scanned at a rate of ~100 pixels per second. Valence-loss spectra were acquired from particles and particle clusters in random orientations. The spectra were similar suggesting that orientation effects were not prominent in part because of the large convergence and collection angles employed. The thickness of all investigated samples was under 0.8 mean free paths as estimated from low loss data [34]. The low sample thickness at the specified collection conditions ensured negligible Cherenkov losses. Using a power-law fit, the tail of the zero-loss peak was removed and the band gap was extracted according to the linear fit method [35].

Core-loss EELS data were acquired on the same instrument as the valence-loss EELS. A monochromated STEM mode was used with dispersions of 10 and 25 meV/channel for Ti and O edges respectively. The convergence angle was 37 mrad and the collection angle was 23 mrad. An energy resolution of 0.45 eV as determined by the FWHM of the ZLP, was obtained. The probe was scanned at a rate of ~200 pixels per second. The background and plural scattering were removed using a standard power law fit and Fourier-ratio deconvolution respectively [36]. Then spectra of each polymorph were fitted with Hartree–Slater ionization cross-section and a total of seven/two Pseudo-Voigt profiles for Ti $L_{3,2}$/O K edges respectively. R^2 for all fits was above 0.997 (see supporting information, Fig. S3). The Hartree-Slater cross section was calculated based on tabulations of the generalized oscillator strength (GOS) with GMS 3.5 software following the approach of Leapman et al. [37] and Ahn et al. [38]. Convergence angle correction was included directly within the GOS integral over momentum transfer by means of the "aperture cross--correlation" method developed by Kohl [39].

All EELS data were taken using dual-channel acquisition [40] and electron spectroscopy imaging (ESI) techniques. Imaging and spectroscopy data were collected using a high-angle annular dark field (HAADF) detector and a GIF Quantum ER spectrometer respectively. Spectroscopic data was gain averaged by the natural spectral shift of the monochromated beam and thus had high signal-to-noise ratio (SNR) [41].The spectra within each spectrum-image data-set were aligned using the ZLP. Outlying spectral values (X-ray spikes) were set to local median values. The spectra reported in this work correspond to summations over thin areas of samples (areas without carbon film and with sample thickness <30 nm).

UV-VIS diffuse reflectance spectroscopy. UV-VIS diffuse reflectance measurements were performed at room temperature on finely ground samples. Spectra were recorded in the range from 200 to 800 nm with an Agilent Cary 5000 UV-VIS-NIR spectrometer equipped with a diffuse reflectance accessory from Harrick. A polytetrafluoroethylene (PTFE) pellet (100% reflectance) was used as the reference. Band gap values were approximated from linear extrapolation to zero of Kubelka-Munk function, $[F(r)\cdot h\upsilon]^n$, plotted against photon energy (Tauc plots) [42–45]. Exponent n equal to 2 and ½ was used for direct and indirect allowed transitions, respectively. For comparison purposes, all Tauc plots were arbitrarily normalized.

3. Results and discussion

3.1. Structural relations

The structures of the four TiO_2 polymorphs anatase, brookite, rutile, and TiO_2-II are all based on octahedral TiO_6 units. They have been described and related numerous times [2,46], and we only provide a summary. Anatase and rutile are tetragonal (space groups $I4_1/amd$ and $P4_2/mnm$, respectively) and brookite and TiO_2-II are orthorhombic (space groups *Pbca* and *Pbcn*, respectively). The local symmetry of TiO_6 polyhedra decreases from D_{4d} (anatase), D_{2h} (rutile), C_2 (TiO_2-II), to C_1 (brookite). All structures can be considered as being built from chains of edge-condensed TiO_6 units. In anatase these chains correspond either to zigzag chains along the [100] direction or screws along the 4_1 axes in the tetragonal crystal structure (we chose the latter, Fig. 1a). In brookite and TiO_2-II they correspond to zigzag chains along the orthorhombic c direction (Fig. 1b and c), and in rutile they correspond to linear chains that run along the tetragonal c direction (Fig. 1d). The distance between Ti atoms in these chains is around 3 Å.

The chains are connected to neighboring ones through common octahedron edges and/or corners. Corner sharing results in next-nearest Ti–Ti neighbors at two distinct distances, around 3.5 Å when Ti–*O*–Ti angles are bent (around 130°) and 3.8 Å when Ti–*O*–Ti angles are close to linear (around 160°). The latter situation arises only in conjunction with simultaneous edge connectivity. In anatase chains are connected so that each octahedron shares edges with two octahedra from different adjacent chains (same short Ti–Ti distance, 3 Å), Fig. 1a. In addition, each octahedron experiences (linear) corner connectivity with octahedra from neighboring chains at a Ti–Ti distance ~3.8 Å (Fig. 1a). In brookite zigzag chains – located as isolated moieties in layers A, B, C, D parallel to the *bc* plane – are alternately connected via common corners ("bent connectivity") and edges to adjacent layers (AcBeCcDeA) along the orthorhombic *a* direction (Fig. 1b). (Lower case letters c and e refer to corner-end edge-connectivity, respectively). Again, the edge-link introduces a short Ti–Ti contact (2.95 Å), and in the edge-linked layer there are in addition two linear corner-connections (3.79 Å) (Fig. 1).

The TiO_2-II structure is topologically very similar to brookite, only that adjacent layers are exclusively connected via common corners, i.e. AcBcA (Fig. 1c). Rutile is built from layers containing linear strands which are connected via common corners. Thus, TiO_2-II is also closely related to rutile and the relationship has been described in detail by Andersson and Galy [47]. Density increases by about 12% across the series anatase (3.895 g/cm^3) – brookite (4.13 g/cm^3, +6%) – rutile (4.274 g/cm^3, +3.5%) – TiO_2-II (4.35 g/cm^3, +1.8%).

3.2. Core-loss EELS analysis

Core-loss EELS refers to the creation of a core hole via excitation of an inner shell electron due to perturbations caused by highly energetic primary electrons generated in the TEM. In titana, the transitions of interest for this study include electrons from the Ti 2*p* shell to unoccupied 3*d* orbitals (Ti $L_{3,2}$ edge) or electrons from a O 1*s* shell to the 2*p* orbital that is hybridized with the Ti 3*d* states (O *K* edge). Ti $L_{3,2}$ ELNES spectra of the four polymorphs obtained by us are shown in Fig. 2. Anatase and rutile have been investigated numerous times and our spectra are in good agreement with previous EELS [33,48–54] and high-resolution XAS

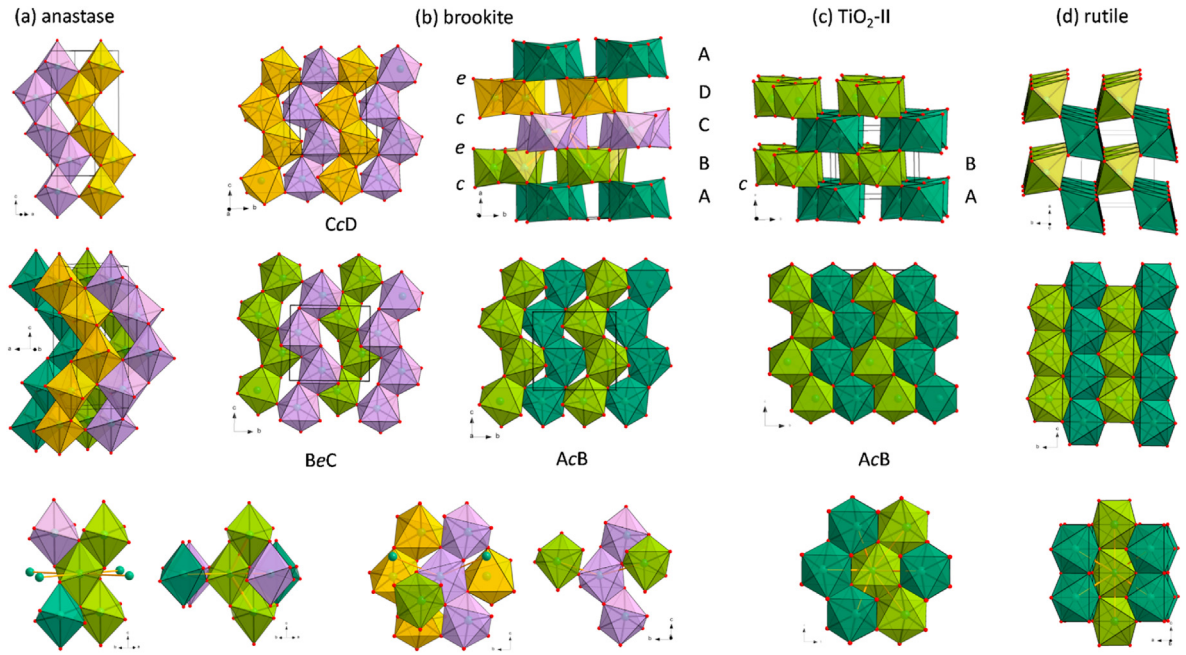

Fig. 1. Crystal structures of anastase (a), brookite (b), TiO_2-II (c), and rutile (d). The first two rows show the chains of edge-condensed TiO_6 octahedra as building units and their connectivity. Capital letters in (b) and (c) denote layers containing building units and lower case letters denote their connectivity, corner and edge-condensed. The bottom row emphasizes the connectivity of a TiO_6 unit (within a chain fragment of three octahedra) with neighboring ones. For clarity, the linear corner-links in anatase and brookite ($d_{Ti\text{-}Ti} \approx 3.8$ Å) are depicted as two figures, one showing only the Ti atoms (green spheres) of linear corner-linked octahedra (left) and one that only shows the octahedra of linear corner links (i.e. the octahedra of the other links were removed, right).

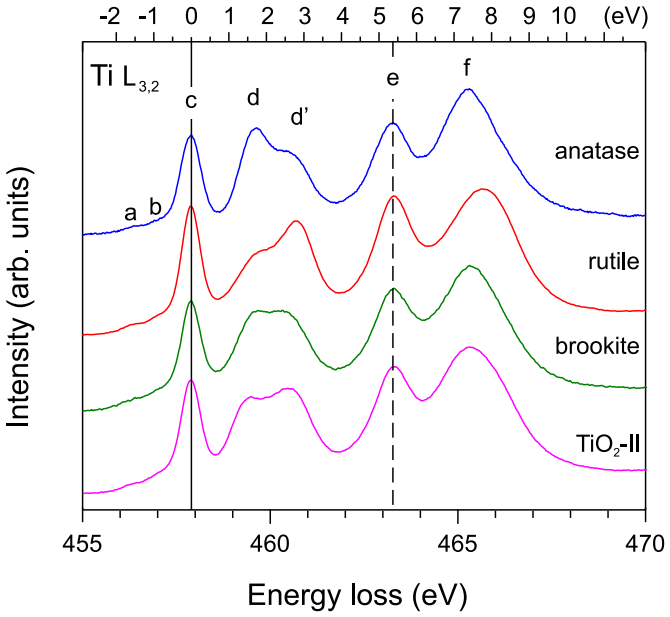

Fig. 2. Ti $L_{3,2}$ ELNES spectrum of TiO_2-II in comparison with anatase, rutile and brookite. The upper axis depicts energies relative to the "c" whiteline of the L_3 edge.

studies, [49,55–57]. Ti 2*p* XAS and $L_{3,2}$ ELNES spectra are characterized by four white lines, here labelled c, d, e, f with increasing energy loss. The low intensity pre-peaks a, b are usually attributed to spin-forbidden transitions [54,56]. The (c,d) and (e,f) doublets reflect the L_3 and L_2 edges, respectively, separated by the ~5.5 eV spin-orbit coupling of the Ti 2*p* core electrons, whereas the doublet feature reflects the octahedral $t_{2g} - e_g$ crystal field splitting (about 2 eV). However, note that because of the intricacies of the Ti 2*p* core hole (many electron and multiplet (correlation) effects due to strong Coulomb interactions between poorly screened 3*d* electrons and 2*p* core hole) [50,57,58], the "true" $t_{2g} - e_g$ splitting is rather extracted from the O *K* edge, see analysis below.

Most important is the split of the L_3 e_g peak (into d and d'), which may reveal additional fine-structuring in very high energy resolution experiments (<0.2 eV) [59]. This d,d' splitting does not seem to be connected to the symmetry lowering of the octahedral environment from O_h to D_{2h} (for which its size, about 1 eV, is simply too large) [54,60], but rather expresses long range band/crystal structure effects, i.e., is caused by next nearest neighbor interactions [59,61]. Directly calculating Ti $L_{3,2}$ ELNES spectra from first principles for more detailed interpretation remains notoriously difficult [27,58].

Differences in the d,d' split feature is the most significant variation in the Ti $L_{3,2}$ ELNES spectra of TiO_2 polymorphs. Despite the lack of a fundamental explanation it has been suggested that the d,d' split feature should allow for unambiguous discrimination of TiO_2 polymorphs [53] and spatially resolved EELS is being increasingly applied for the analysis of nanocrystalline multiphase samples [28,62], core-shell structures [31] or grain boundary structures [27,33]. The largest d,d' difference is seen for rutile and anatase, where intensities seem reversed. For brookite d,d' intensities appear roughly equal, and TiO_2-II places itself between brookite and rutile. In order to make a meaningful comparison, we fitted the seven spectral constituents a – f with Pseudo-Voigt functions. A similar strategy was applied by Ruus et al. for the evaluation of XAS spectra [55]. The results are shown in Table 1, for details see Method section and Fig. S3. With this, the differences between the spectra become more quantitative. The key information is summarized in Table 2: (i) The intensity ratio of the L_3 e_g split (d/d') is very similar for brookite and TiO_2-II (around 0.42) whereas it is considerably larger for rutile and anatase (around 0.7). (Note, that the crude inspection of d,d' intensities suggested a large difference between rutile and anatase). (ii) The size of the e_g split is very similar for rutile and TiO_2-II (around 1.15 eV) whereas it is considerably smaller for anatase and brookite (around 0.96 eV). (iii) The intensity ratio of the L_3 $t_{2g} - e_g$ split (c/(d + d')) increases along TiO_2-II – brookite – anatase – rutile.

As initially indicated, the d,d' split reflects electronic/crystal

Table 1
Positions, areas and FWHM (in eV) of Ti and O ELNES profile features of anatase, rutile, brookite and TiO_2-II. All positions are relative to the strongest feature of the respective edge. All areas are normalized with respect to c and A, respectively.

	Anatase			Rutile			Brookite			TiO_2-II		
Ti $L_{3,2}$ edge												
	position	area	FWHM	position	area	FWHM	position	area	FWHM	position	area	FWHM
a	−1.42(8)	0.10(2)	0.42(9)	−1.44(5)	0.12(2)	0.45(5)	−1.40(5)	0.20(3)	0.54(5)	−1.37(7)	0.13(2)	0.46(7)
b	−0.85(2)	0.06(2)	0.19(3)	−0.85(1)	0.07(1)	0.21(2)	−0.84(1)	0.09(2)	0.21(2)	−0.82(2)	0.09(2)	0.22(3)
c	0.000(2)	1.000(8)	0.29(1)	0.000(1)	1.000(5)	0.29(1)	0.000(1)	1.000(6)	0.31(1)	0.000(1)	1.000(6)	0.30(1)
d	1.663(5)	1.16(4)	0.40(1)	1.70(1)	1.04(2)	0.64(1)	1.541(9)	0.90(5)	0.52(1)	1.447(5)	0.94(2)	0.49(1)
d'	2.60(1)	1.67(4)	0.68(1)	2.843(6)	1.54(2)	0.59(1)	2.52(2)	2.15(5)	0.81(1)	2.596(7)	2.22(3)	0.77(1)
e	5.271(3)	1.83(1)	0.56(1)	5.360(2)	2.075(9)	0.65(1)	5.296(2)	1.98(1)	0.65(1)	5.305(2)	1.85(1)	0.61(1)
f	7.462(3)	4.84(3)	1.02(1)	7.760(2)	4.13(2)	1.09(1)	7.496(2)	4.50(2)	1.07(1)	7.522(3)	4.89(2)	1.16(1)
O *K* edge												
	position	area	FWHM	position	area	FWHM	position	area	FWHM	position	area	FWHM
A	0.000(2)	1.000(5)	0.72(1)	0.000(3)	1.000(6)	0.75(1)	0.000(3)	1.000(7)	0.77(1)	0.000(3)	1.000(6)	0.75(1)
B	2.613(3)	1.51(2)	1.02(1)	2.820(4)	1.77(2)	0.97(1)	2.653(4)	1.94(4)	1.17(2)	2.694(4)	1.69(2)	1.06(1)

Table 2
Relations between some Ti and O ELNES features for anatase, rutile, brookite and TiO_2-II.

	feature	Anatase	Rutile	Brookite	TiO_2-II
d/d'	Ti L_3	0.70(8)	0.68(5)	0.42(1)	0.42(6)
(d'-d)		0.94(1)	1.14(1)	0.98(2)	1.15(1)
c/(d + d')		0.35(6)	0.39(4)	0.33(7)	0.32(3)
(f-e)	Ti L_2	2.191(5)	2.400(3)	2.200(3)	2.217(3)
(B-A)	O *K* (true t_{2g}-e_g)	2.613(4)	2.820(5)	2.653(6)	2.694(5)

structure differences of the polymorphs stemming from next nearest neighbor interactions, i.e. of the octahedral chain structural unites (cf. Fig. 1). Given the structural similarity of TiO_2-II to both brookite and rutile it is then not surprising that quantification of the split feature would reveal similarities to these polymorphs.

The O *K* ELNES spectra of the four polymorphs are shown in Fig. 3. Here differences between the polymorphs are much less apparent. As mentioned above, the two main peaks (A, B) reflect the "true" t_{2g} – e_g spitting of the polymorphs. Here TiO_2-II (2.69 eV) aligns with anatase and brookite (2.61 and 2.65 eV, respectively), whereas the splitting is distinctly larger for rutile (2.82 eV), cf. Table 2 [54,55]. A second set of bands is seen in the 537–548 eV range. In the octahedral MO picture, these transitions involve higher lying (antibonding) a_{1g} (Ti4*s*-O2*p*-σ) and t_{1u} (Ti4*p*-O2*p*-π) states [52,54]. The latter would split into two and three components for tetragonal and orthorhombic distortions, respectively. Apparently, the MO picture does not describe fully the features of the O *K* ELNES spectra. In contrast with Ti $L_{3,2}$ ELNES spectra O *K* spectra can be computed highly satisfactorily from first principles calculations of the O 2*p*-projected unoccupied DOS (above the Fermi level) [54]. Here we would expect greatest similarities for orthorhombic TiO_2-II and brookite.

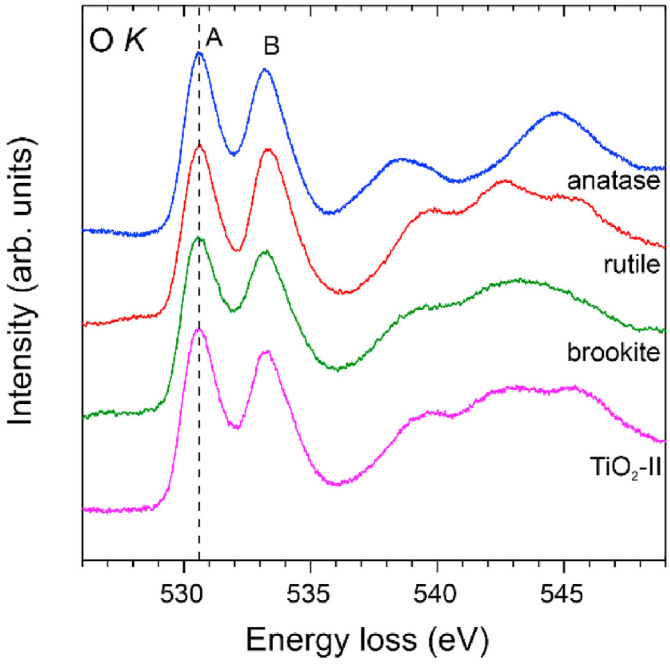

Fig. 3. O *K* ELNES spectrum of TiO_2-II in comparison with anatase, rutile and brookite.

3.3. Band gap analysis

The size and nature (direct or indirect) of the band gap for rutile and anatase are widely reported in the literature [28,44,63,64]. For brookite reports are much more sparse and also more inconsistent [64–69]. For TiO_2-II information is essentially limited to computational findings [24,25], apart from a recent thin film study [23]. Generally, reported band gaps scatter somewhat depending on the particle size and morphology of the polymorphs, but also on the measurement method and data analysis for band gap extraction [44,45,64]. It appears established that rutile has a direct band gap of ~3.0 eV and anatase an indirect band gap of ~3.2 eV. Brookite, in the form of thin films, was reported with a direct band gap of ~3.45 eV [69]. DFT electronic structure calculations indicate an indirect band gap with a size around 2.63 eV (using LDA and GGA functionals) [24,25] or 4.09 eV (using the B3LYP functional) [25].

UV-VIS diffuse reflectance spectroscopy is limited for band gap determination when it comes to strongly absorbing materials. The Kubelka-Munk (KM) theory used for the evaluation of reflectance spectra assumes a linear relationship between intrinsic scattering and absorption coefficients (s and α) and theoretical ones (usually denoted as S and K respectively), which is not the case for strongly absorbing materials [70,71]. Certain corrections can be made to the KM function [44,71,72], but their use is often not properly reported, leading to discrepancies in the published data. In this paper, we use the unmodified KM function. Band gap studies using valence loss EELS data can be challenging because multiple scattering deconvolution, nonzero collection angle correction and removal of zero loss peak (ZLP) need to be correctly performed during data reduction steps [73–77]. Proper beam monochromation for easier ZLP removal, aberration correction for best spatial resolution and careful choice of data collection area on a sample for minimization of Cherenkov radiation help to achieve best energy and spatial resolution of the data and thus allow relatively precise bad gap determination.

Fig. 4 shows the valence loss EELS spectra of the four polymorphs and Fig. 5 shows the KM function F(R) extracted from the diffuse reflectance

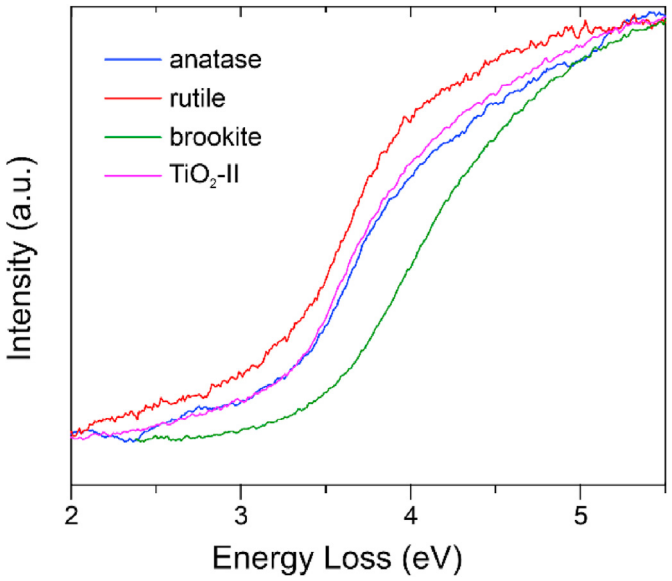

Fig. 4. Low loss EELS spectra of TiO_2-II in comparison with anatase, rutile and brookite.

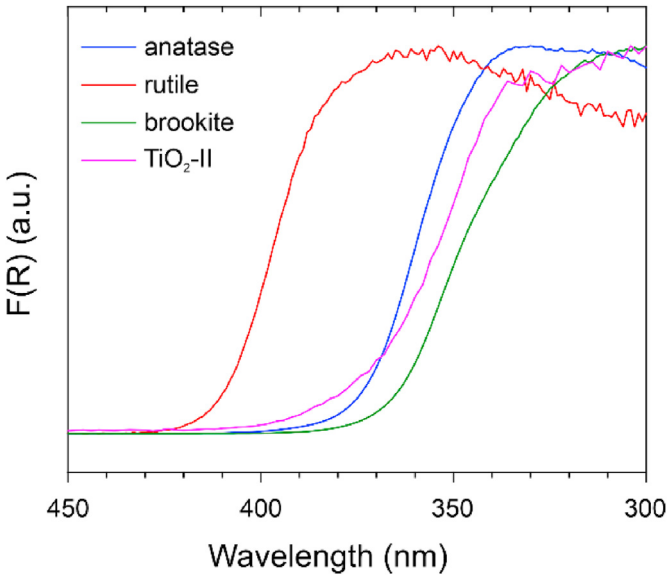

Fig. 5. Kubelka-Munk function $F(R) = (1 - R^2)/2R$ (where R = reflectance) of bulk TiO_2-II in comparison with anatase, rutile and brookite.

UV-VIS measurements. $F(R) = (1\text{-}R)^2/2R$ represents a pseudo absorption coefficient [42]. The band gap from the valence loss EELS spectra was obtained with the intersection of a linear fit to the intensity rise and x-axis after ZLP and background removal as described in the Methods section. The band gap from the UV-VIS spectra was obtained from Tauc plots and considering both an indirect and a direct allowed transition case (see supporting information, Fig. S4, for detailed information). The band gaps are compiled in Table 3. One recognizes excellent agreement between the valence loss EELS and UV-VIS gaps when assuming indirect band gaps for anatase and TiO_2-II and direct band gaps for rutile and brookite. The band gap of TiO_2-II (indirect, ~3.18 eV) is slightly narrower than that of anatase (indirect, ~3.2 eV). Our (bulk) value is lower than that reported for TiO_2-II thin films (3.28–3.36 eV) [23]. Band gaps for both anatase and rutile are broadly consistent with widely reported literature values (indirect ~3.2 and direct ~3.05 eV respectively). The band gap for brookite was confirmed to be the largest among titania polymorphs studied here (direct, ~3.45 eV) and agrees with reported values for both brookite thin films and nanocrystals (reported as direct ~3.45 eV and indirect ~3.40 eV respectively) [66,69].

Table 3
Band gap values (in eV) for anatase, rutile, brookite and TiO_2-II extrapolated from EELS spectra, the Kubelka-Munk function F(R), and Tauc plots (calculated for direct and indirect allowed transitions). Bold numbers refer to the proper assignment of direct and indirect band gap.

	EELS	F(R)	UV-VIS direct	UV-VIS indirect
Anatase	3.20(2)	3.30(1)	3.40(1)	**3.22(2)**
Rutile	3.09(2)	3.00(2)	**3.07(3)**	2.99(3)
Brookite	3.44(1)	3.37(2)	**3.48(3)**	3.28(1)
TiO_2-II	3.18(2)	3.29(3)	3.45(5)	**3.20(5)**

4. Conclusions

The electronic structure and band gap of TiO_2-II with the α-PbO_2 structure was characterized with EELS and UV-VIS diffuse reflectance spectroscopy. High resolution valence-loss and core-loss EELS data were acquired in monochromated STEM mode on a probe and image aberration corrected microscope. This system enabled the recording of spectra with an energy resolution of about 0.2 eV thus providing detailed near-edge fine structure and band gap data alongside with nanometer scale image resolution. The titanium $L_{3,2}$ and oxygen *K* electron ELNES spectra of TiO_2-II show a strong similarity with both rutile and brookite, which reflects similarities in the connectivity of octahedral TiO_6 units with neighboring ones. Although ELNES differences of TiO_2 are rather small they appear distinct enough for the high precision nanophase mapping, core-shell or grain boundary studies of mixed phase samples. The band gap of TiO_2-II was determined to be indirect and with a size of about 3.18 eV, which is very similar to anatase (indirect, ~3.2 eV), suggesting that TiO_2-II possesses a similarly high photocatalytic activity as anatase. Both forms are clearly distinguished from rutile and brookite which have direct band gaps with sizes ~3.05 and 3.45 eV, respectively.

CRediT authorship contribution statement

Alisa Gordeeva: Conceptualization, Investigation, Data curation, Writing – original draft. **Thomas Thersleff:** Methodology, Validation, Writing – review & editing. **Ying-Jui Hsu:** Investigation, Visualization. **Christian Liebske:** Investigation, Methodology. **Peter Ulmer:** Investigation, Methodology. **Ove Andersson:** Investigation, Writing – review & editing. **Ulrich Häussermann:** Funding acquisition, Project administration, Supervision, Writing – review & editing.

Declaration of competing interest

The authors declare that they have no known competing financial interests or personal relationships that could have appeared to influence the work reported in this paper.

Data availability

Data will be made available on request.

Acknowledgement

This work was funded by The Swedish Research Council (Grant 2016-04413). Additionally we gratefully acknowledge the support from Stiftelsen Olle Engkvist Byggmästare (YJH).

Appendix A. Supplementary data

Supplementary data to this article can be found online at https://doi.org/10.1016/j.jssc.2023.123952.

References

[1] A.A. Levchenko, G. Li, J. Boerio-Goates, B.F. Woodfield, A. Navrotsky, TiO_2 stability landscape: polymorphism, surface energy, and bound water energetics, Chem. Mater. 18 (26) (2006) 6324–6332, https://doi.org/10.1021/cm061183c.

[2] H. Zhang, J.F. Banfield, Structural characteristics and mechanical and thermodynamic properties of nanocrystalline TiO_2, Chem. Rev. 114 (2014) 9613–9644, https://doi.org/10.1021/cr500072j.

[3] X. Chen, S.S. Mao, Titanium dioxide nanomaterials: synthesis, properties, modifications and applications, Chem. Rev. 107 (7) (2007) 2891–2959, https://doi.org/10.1021/cr0500535.

[4] M. Cargnello, T.R. Gordon, C.B. Murray, Solution-phase synthesis of titanium dioxide nanoparticles and nanocrystals, Chem. Rev. 114 (19) (2014) 9319–9345, https://doi.org/10.1021/cr500170p.

[5] A. Fujishima, X. Zhang, Titanium dioxide photocatalysis: present situation and future approaches, Compt. Rendus Chem. 9 (5–6) (2006) 750–760, https://doi.org/10.1016/j.crci.2005.02.055.

[6] K. Nakata, A. Fujishima, TiO_2 photocatalysis: design and applications, J. Photochem. Photobiol. C Photochem. Rev. 13 (3) (2012) 169–189, https://doi.org/10.1016/j.jphotochemrev.2012.06.001.

[7] R. Verma, J. Gangwar, A.K. Srivastava, Multiphase TiO_2 nanostructures: a review of efficient synthesis, growth mechanism, probing capabilities, and applications in biosafety and health, RSC Adv. 7 (70) (2017) 44199–44224, https://doi.org/10.1039/c7ra06925a.

[8] N.A. Bendeliani, S.V. Popova, L.F. Vereshchagin, New modification of titanium dioxide obtained at high pressures, Geochem. Int. 3 (1966) 387–390.

[9] P.Y. Simons, F. Dachille, The structure of TiO_2 II, a high-pressure phase of TiO_2, Acta Crystallogr. 23 (2) (1967) 334–336, https://doi.org/10.1107/s0365110x67002713.

[10] A.C. Withers, E.J. Essene, Y. Zhang, Rutile/TiO_2II phase equilibria, Contrib. Mineral. Petrol. 145 (2) (2003) 199–204, https://doi.org/10.1007/s00410-003-0445-2.

[11] K. Spektor, D.T. Tran, K. Leinenweber, U. Häussermann, Transformation of rutile to TiO_2-II in a high pressure hydrothermal environment, J. Solid State Chem. 206 (2013) 209–216, https://doi.org/10.1016/j.jssc.2013.08.018.

[12] A. Gordeeva, Y.-J. Hsu, T. Thersleff, I.Z. Jenei, C. Liebske, P. Ulmer, M. Antlauf, O. Andersson, U. Haussermann, Stability fields of TiO_2 polymorphs from crystallization of amorphous titania in hydrothermal environments from ambient pressure to 5 GPa, Unpubl. Manuscr. (2023).

[13] W. Yong, E. Dachs, A. Benisek, R.A. Secco, Heat capacity and entropy of rutile and TiO_2II: thermodynamic calculation of rutile-TiO_2II transition boundary, Phys. Earth Planet. In. 226 (2014) 39–47, https://doi.org/10.1016/j.pepi.2013.10.004.

[14] H. Kojitani, M. Yamazaki, M. Kojima, Y. Inaguma, D. Mori, M. Akaogi, Thermodynamic investigation of the phase equilibrium boundary between TiO_2 rutile and its α-PbO_2-type high-pressure polymorph, Phys. Chem. Miner. 45 (2018) 963–980, https://doi.org/10.1007/s00269-018-0977-7.

[15] Z. Tan, P. Chen, Q. Zhou, J. Liu, X. Mei, B. Wang, N. Cui, Shock synthesis and characterization of titanium dioxide with α-PbO_2 structure, J. Phys. Condens. Matter 30 (26) (2018), https://doi.org/10.1088/1361-648X/aac709.

[16] S. Wu, W. Wang, W. Tu, S. Yin, Y. Sheng, M.Y. Manuputty, M. Kraft, R. Xu, Premixed stagnation flame synthesized TiO_2 nanoparticles with mixed phases for efficient photocatalytic hydrogen generation, ACS Sustain. Chem. Eng. 6 (11) (2018) 14470–14479, https://doi.org/10.1021/acssuschemeng.8b03142.

[17] M.Y. Manuputty, J.A.H. Dreyer, Y. Sheng, E.J. Bringley, M.L. Botero, J. Akroyd, M. Kraft, Polymorphism of nanocrystalline TiO_2 prepared in a stagnation flame: formation of the TiO_2-II phase, Chem. Sci. 10 (5) (2019) 1342–1350, https://doi.org/10.1039/c8sc02969e.

[18] S. Sen, M.L. Ram, S. Roy, B.K. Sarkar, The structural transformation of anatase TiO_2 by high-energy vibrational ball milling, J. Mater. Res. 200 (1999) 841–848, https://doi.org/10.1557/JMR.1999.0112.

[19] M.G. Rinaudo, A.M. Beltrán, M.A. Fernández, L.E. Cadús, M.R. Morales, Tailoring materials by high-energy ball milling: TiO_2 mixtures for catalyst support application, Mater. Today Chem. 17 (2020) 1–13, https://doi.org/10.1016/j.mtchem.2020.100340.

[20] I.E. Grey, C. Li, I.C. Madsen, G. Braunshausen, TiO_2-II. Ambient pressure preparation and structure refinement, Mater. Res. Bull. 23 (5) (1988) 743–753, https://doi.org/10.1016/0025-5408(88)90040-2.

[21] J. Aarik, A. Aidla, V. Sammelselg, H. Siimon, T. Uustare, Control of thin film structure by reactant pressure in atomic layer deposition of TiO_2, J. Cryst. Growth 169 (3) (1996) 496–502, https://doi.org/10.1016/S0022-0248(96)00423-X.

[22] A. Tarre, K. Möldre, A. Niilisk, H. Mändar, J. Aarik, A. Rosental, Atomic layer deposition of epitaxial TiO_2 II on c-sapphire, J. Vac. Sci. Technol. A Vacuum, Surfaces, Film. 31 (1) (2013), 01A118, https://doi.org/10.1116/1.4764892.

[23] K. Möls, L. Aarik, H. Mändar, A. Kasikov, A. Niilisk, R. Rammula, J. Aarik, Influence of phase composition on optical properties of TiO_2: dependence of refractive index and band gap on formation of TiO_2-II phase in thin films, Opt. Mater. 96 (2019), 109335, https://doi.org/10.1016/j.optmat.2019.109335.

[24] M.Y. Kuo, C.L. Chen, C.Y. Hua, H.C. Yang, P. Shen, Density functional theory calculations of dense TiO_2 polymorphs: implication for visible-light-responsive photocatalysts, J. Phys. Chem. B 109 (2005) 8693–8700, https://doi.org/10.1021/jp0510903.

[25] Q.J. Liu, N.C. Zhang, F.S. Liu, Z.T. Liu, Structural, elastic, electronic and optical properties of various mineral phases of TiO_2 from first-principles calculations, Phys. Scripta 89 (7) (2014), https://doi.org/10.1088/0031-8949/89/7/075703, 075703–075717.

[26] T. Zhu, S.P. Gao, The stability, electronic structure, and optical property of TiO_2 polymorphs, J. Phys. Chem. C 118 (2014) 11385–11396, https://doi.org/10.1021/jp412462m.

[27] G. Schusteritsch, R. Ishikawa, A.R. Elmaslmane, K. Inoue, K.P. McKenna, Y. Ikuhara, C.J. Pickard, Anataselike grain boundary structure in rutile titanium dioxide, Nano Lett. 21 (7) (2021) 2745–2751, https://doi.org/10.1021/acs.nanolett.0c04564.

[28] D.M. Tobaldi, L. Lajaunie, N. Rozman, A.P.F. Caetano, M.P. Seabra, A. Sever Škapin, R. Arenal, J.A. Labrincha, Impact of the absolute rutile fraction on TiO_2 visible-light absorption and visible-light-promoted photocatalytic activity, J. Photochem. Photobiol. Chem. 382 (2019), 111940, https://doi.org/10.1016/j.jphotochem.2019.111940.

[29] M. Tian, C. Liu, J. Ge, D. Geohegan, G. Duscher, G. Eres, Recent progress in characterization of the core-shell structure of black titania, J. Mater. Res. 34 (7) (2019) 1138–1153, https://doi.org/10.1557/jmr.2019.46.

[30] H.-S. Seo, H.S. Park, Fabrication and characterization of Ti and TiO_2 nanoparticles by pulsed wire evaporation and transmission electron microscopy, J. Nanosci. Nanotechnol. 18 (10) (2018) 6823–6829, https://doi.org/10.1166/jnn.2018.15452.

[31] M. Tian, M. Mahjouri-samani, G. Eres, R. Sachan, M. Yoon, M.F. Chisholm, K. Wang, A.A. Puretzky, C.M. Rouleau, D.B. Geohegan, G. Duscher, Structure and formation mechanism of black TiO_2 nanoparticles, ACS Nano 10 (2015) 10482–10488, https://doi.org/10.1021/acsnano.5b04712.

[32] G. Bertoni, E. Beyers, J. Verbeeck, M. Mertens, P. Cool, E.F. Vansant, G. Van Tendeloo, Quantification of crystalline and amorphous content in porous TiO_2 samples from electron energy loss spectroscopy, Ultramicroscopy 106 (7) (2006) 630–635, https://doi.org/10.1016/j.ultramic.2006.03.006.

[33] L. Casanova, M. Arosio, M. Taghi Hashemi, M.P. Pedeferri, G.A. Botton, M. Ormellese, A nanoscale investigation on the influence of anodization parameters during plasma electrolytic oxidation of titanium by high-resolution electron energy loss spectroscopy, Appl. Surf. Sci. 570 (September) (2021), 151133, https://doi.org/10.1016/j.apsusc.2021.151133.

[34] T. Malis, S.C. Cheng, R.F. Egerton, EELS log-ratio technique for specimen-thickness measurement in the TEM, J. Electron. Microsc. Tech. 8 (2) (1988) 193–200, https://doi.org/10.1002/jemt.1060080206.

[35] J. Park, SungHeo, J. Chung, H. Kim, G. Park, Bandgap measurement of dielectric thin films by using monochromated STEM-EELS, Microsc. Microanal. 13 (2007) 1306–1307, https://doi.org/10.1017/S1431927607075411.

[36] R.F. Egerton, Electron energy-loss spectroscopy in the TEM, Rep. Prog. Phys. 72 (2009), https://doi.org/10.1088/0034-4885/72/1/016502, 016502–016527.

[37] R.D. Leapman, P. Rez, D.F.K.L. Mayers, M. Shell, Generalized oscillator strengths and ionization cross sections for fast electron collisions, J. Chem. Phys. 72 (1980) 1232–1243, https://doi.org/10.1063/1.439184.

[38] C. Ahn, P. Rez, Inner shell edge profiles in electron energy loss spectroscopy, Ultramicroscopy 17 (1985) 105–116, https://doi.org/10.1016/0304-3991(85)90003-8.

[39] H. Kohl, A simple procedure for evaluating effective scattering cross-section in STEM, Ultramicroscopy 16 (1985) 265–268, https://doi.org/10.1016/0304-3991(85)90081-6.

[40] J. Scott, P.J. Thomas, M. Mackenzie, S. Mcfadzean, J. Wilbrink, A.J. Craven, W.A.P. Nicholson, Near-simultaneous dual energy range EELS spectrum imaging, Ultramicroscopy 108 (2008) 1586–1594, https://doi.org/10.1016/j.ultramic.2008.05.006.

[41] M. Bosman, V.J. Keast, Optimizing EELS acquisition, Ultramicroscopy 108 (9) (2008) 837–846, https://doi.org/10.1016/j.ultramic.2008.02.003.

[42] P. Kubelka, F.A. Munk, Contribution to the optics of pigments, Z. Technol. Phys. 12 (1931) 593–599.

[43] J. Tauc, R. Grigorovici, A. Vancu, Optical properties and electronic structure of amorphous germanium, Phys. Status Solidi 15 (1966) 627–637, https://doi.org/10.1002/pssb.19660150224.

[44] R. Lopez, R. Gomez, Band-gap energy estimation from diffuse reflectance measurements on sol – gel and commercial TiO_2: a comparative study, J. Sol. Gel Sci. Technol. 61 (2012) 1–7, https://doi.org/10.1007/s10971-011-2582-9.

[45] P. Makuła, M. Pacia, W. Macyk, How to correctly determine the band gap energy of modified semiconductor photocatalysts based on UV−Vis spectra, J. Phys. Chem. Lett. 9 (2018) 6814–6817, https://doi.org/10.1021/acs.jpclett.8b02892.

[46] Z. Hiroi, Inorganic structural chemistry of titanium dioxide polymorphs, Inorg. Chem. 61 (2022) 8393–8401, https://doi.org/10.1021/acs.inorgchem.2c00945.

[47] S. Andersson, J. Galy, Terms and conditions privacy policy copyright © 2022 elsevier B.V. All rights reserved. Scopus® is a registered trademark of elsevier B.V, Bull. Soc. Chim. Fr. 4 (1969) 1065–1066.

[48] R. Brydson, B.G. Williams, W. Engel, H. Sauer, E. Zeitler, J.M. Thomas, Electron energy-loss spectroscopy (EELS) and the electronic structure of titanium dioxide, Solid State Commun. 64 (4) (1987) 609–612, https://doi.org/10.1016/0038-1098(87)90792-7.

[49] R. Brydson, H. Sauer, W. Engel, J.M. Thomass, E. Zeitler, N. Kosugi, H. Kuroda, Electron energy loss and X-ray absorption spectroscopy of rutile and anatase: a test of structural sensitivity, J. Phys. Condens. Matter 1 (4) (1989) 797–812, https://doi.org/10.1088/0953-8984/1/4/012.

[50] F.M.F. de Groot, J.C. Fuggle, B.T. Thole, G.A. Sawatzky, $L_{2,3}$ X-ray- absorption edges of d^0 compounds: K^+, Ca^{2+}, Sc^{3+} and Ti^{4+} in O_h (octahedral) symmetry, Phys. Rev. B 41 (2) (1990) 928–937, https://doi.org/10.1103/PhysRevB.41.928.

[51] R. Brydson, H. Sauer, W. Engel, F. Hofer, Electron energy-loss near-edge structures at the oxygen K edges of titanium(IV) oxygen compounds, J. Phys. Condens. Matter 4 (13) (1992) 3429–3437, https://doi.org/10.1088/0953-8984/4/13/007.

[52] C. Mitterbauer, G. Kothleitner, W. Grogger, H. Zandbergen, B. Freitag, P. Tiemeijer, F. Hofer, Electron energy-loss near-edge structures of 3d transition metal oxides

recorded at high-energy resolution, Ultramicroscopy 96 (2003) 469–480, https://doi.org/10.1016/S0304-3991(03)00109-8.
[53] C. Heiliger, F. Heyroth, F. Syrowatka, H.S. Leipner, I. Maznichenko, K. Kokko, W. Hergert, I. Mertig, Orientation-dependent electron-energy-loss spectroscopy of TiO_2: a comparison of theory and experiment, Phys. Rev. B 73 (4) (2006) 1–8, https://doi.org/10.1103/PhysRevB.73.045129.
[54] E. Stoyanov, F. Langenhorst, G. Steinle-Neumann, The effect of valence state and site geometry on Ti $L_{2,3}$ and O K electron energy-loss spectra of Ti_xO_y phases, Am. Mineral. 92 (4) (2007) 577–586, https://doi.org/10.2138/am.2007.2344.
[55] F.M.F. de Groot, J.C. Fuggle, B.T. Thole, G.A. Sawatzky, 2p X-ray absorption of 3d transition-metal compounds: an atomic multiplet description including the crystal field, Phys. Rev. B 42 (9) (1990) 5459–5468, https://doi.org/10.1117/12.560776.
[56] R. Ruus, A. Kikas, A. Saar, A. Ausmees, E. Nommiste, J. Aarik, A. Aidla, T. Uustare, I. Martinson, Ti 2p and O 1s X-ray absorption of TiO_2 polumorphs, Solid State Commun. 104 (4) (1997) 199–203, https://doi.org/10.1016/S0038-1098(97)00300-1.
[57] S.O. Kucheyev, T. Van Buuren, T.F. Baumann, J.H. Satcher, T.M. Willey, R.W. Meulenberg, T.E. Felter, J.F. Poco, S.A. Gammon, L.J. Terminello, Electronic structure of titania aerogels from soft X-ray absorption spectroscopy, Phys. Rev. B 69 (2004) 1–7, https://doi.org/10.1103/PhysRevB.69.245102.
[58] G. Fronzoni, R. De Francesco, M. Stener, M. Causà, X-ray absorption spectroscopy of titanium oxide by time dependent density functional calculations, J. Phys. Chem. B 110 (20) (2006) 9899–9907, https://doi.org/10.1021/jp057353a.
[59] M. Cheynet, S. Pokrant, S. Irsen, P. Krüger, New fine structures resolved at the ELNES Ti-$L_{2,3}$ edge spectra of anatase and rutile: comparison between experiment and calculation, Ultramicroscopy 110 (2010) 1046–1053, https://doi.org/10.1016/j.ultramic.2010.03.001.
[60] J.P. Crocombette, F. Jollet, Ti 2p X-ray absorption in titanium dioxides (TiO_2): the influence of the cation site environment, Am. Lab. 6 (1994) 10811–10821.
[61] A. Gloter, C. Ewels, P. Umek, D. Arcon, C. Colliex, Electronic structure of titania-based nanotubes investigated by EELS spectroscopy, Phys. Rev. B 80 (2009) 1–6, https://doi.org/10.1103/PhysRevB.80.035413.
[62] T. Thersleff, C.-W. Tai, Feature-specific correlation of structural, optical, and chemical properties in the transmission electron microscope with hypermodal data fusion, Microsc. Microanal. (2022), https://doi.org/10.1093/micmic/ozac018.
[63] H. Tang, H. Berger, P.E. Schmid, F. Levy, D.P. Appliquee, E. Polytechnique, Optical properties of anatase (TiO_2), Solid State Commun. 92 (3) (1994) 267–271, https://doi.org/10.1016/0038-1098(94)90889-3.
[64] D. Reyes-Coronado, G. Rodríguez-Gattorno, M.E. Espinosa-Pesqueira, C. Cab, R. De Coss, G. Oskam, Phase-pure TiO_2 nanoparticles: anatase, brookite and rutile, Nanotechnology 19 (14) (2008) 1–10, https://doi.org/10.1088/0957-4484/19/14/145605.
[65] T. Shibata, H. Irie, M. Ohmori, A. Nakajima, T. Watanabe, K. Hashimoto, Comparison of photochemical properties of brookite and anatase TiO_2 films, Phys. Chem. Chem. Phys. 6 (2004) 1359–1362, https://doi.org/10.1039/b315777f.
[66] M. Koelsch, S. Cassaignon, J.F. Guillemoles, J.P. Jolivet, Comparison of optical and electrochemical properties of anatase and brookite TiO_2 synthesized by the sol-gel method, Thin Solid Films 403–404 (2002) 312–319, https://doi.org/10.1016/S0040-6090(01)01509-7.
[67] A. Di Paola, M. Bellardita, L. Palmisano, Brookite, the least known TiO_2 photocatalyst, Catalysts 3 (2013) 36–73, https://doi.org/10.3390/catal3010036.
[68] T.A. Kandiel, A. Feldhoff, L. Robben, R. Dillert, D.W. Bahnemann, Tailored titanium dioxide nanomaterials: anatase nanoparticles and brookite nanorods as highly active photocatalysts, Chem. Mater. 22 (6) (2010) 2050–2060, https://doi.org/10.1021/cm903472p.
[69] A.M. Alotaibi, S. Sathasivam, B.A.D. Williamson, A. Kafizas, C. Sotelo-Vazquez, A. Taylor, D.O. Scanlon, I.P. Parkin, Chemical vapor deposition of photocatalytically active pure brookite TiO_2 thin films, Chem. Mater. 30 (4) (2018) 1353–1361, https://doi.org/10.1021/acs.chemmater.7b04944.
[70] M. Rundlof, J.A. Bristow, A note concerning the interaction between light scattering and light absorption in the application of the kubelka-munk equations, J. Pulp Pap. Sci. 23 (5) (1997) 220–223.
[71] P. Edström, Examination of the revised kubelka-munk theory: considerations of modeling strategies, J. Opt. Soc. Am. 24 (2) (2007) 548–556, https://doi.org/10.1364/josaa.24.000548.
[72] L. Yang, S.J. Miklavcic, B. Kruse, Qualifying the arguments used in the derivation of the revised kubelka-munk theory: reply, J. Opt. Soc. Am. 24 (2) (2007) 557–560, https://doi.org/10.1364/josaa.24.000557.
[73] R. Erni, N.D. Browning, Valence electron energy-loss spectroscopy in monochromated scanning transmission electron microscopy, Ultramicroscopy 104 (2005) 176–192, https://doi.org/10.1016/j.ultramic.2005.03.009.
[74] L. Gu, V. Srot, W. Sigle, C. Koch, P. Van Aken, F. Scholz, S.B. Thapa, C. Kirchner, M. Jetter, M. Rühle, Band-gap measurements of direct and indirect semiconductors using monochromated electrons, Phys. Rev. B Condens. Matter 75 (19) (2007) 1–8, https://doi.org/10.1103/PhysRevB.75.195214.
[75] R.F. Egerton, Limits to the spatial, energy and momentum resolution of electron energy-loss spectroscopy, Ultramicroscopy 107 (8) (2007) 575–586, https://doi.org/10.1016/j.ultramic.2006.11.005.
[76] M. Stöger-Pollach, Optical properties and bandgaps from low loss EELS: pitfalls and solutions, Micron 39 (8) (2008) 1092–1110, https://doi.org/10.1016/j.micron.2008.01.023.
[77] C.S. Granerød, W. Zhan, Ø. Prytz, Automated approaches for band gap mapping in STEM-EELS, Ultramicroscopy 184 (2018) 39–45, https://doi.org/10.1016/j.ultramic.2017.08.006.